Efficiency of Generalized Regular **k**-point grids

Wiley S. Morgan*, Jeremy J. Jorgensen, Bret C. Hess, Gus L.W. Hart

Department of Physics and Astronomy, Brigham Young University, Provo, UT 84602, USA

ABSTRACT

Most DFT practitioners use regular grids (Monkhorst-Pack, MP) for integrations in the Brillouin zone. Although regular grids are the natural choice and easy to generate, more general grids whose generating vectors are not merely integer divisions of the reciprocal lattice vectors, are usually more efficient (Wisesa et al., 2016). We demonstrate the efficiency of *generalized regular* (GR) grids compared to Monkhorst-Pack (MP) and *simultaneously commensurate* (SC) grids. In the case of metals, for total energy accuracies of one meV/atom, GR grids are 60% faster on average than MP grids and 20% faster than SC grids. GR grids also have greater freedom in choosing the **k**-point density, enabling the practitioner to achieve a target accuracy with the minimum computational cost.

1. Introduction

High throughput materials design has become an effective route to material discovery with many successes already documented [2–31]. The creation of large material databases is the first step in high throughput approaches [32–51]. Computationally expensive electronic structure calculations generate the data for the databases and limit the extent to which data analysis tools, such as machine learning, can be applied. Increasing the speed of these calculations has the potential to significantly increase the size of these databases and the impact of material predictions.

Most electronic structure codes perform numerical integrals over the first Brillouin zone, which converge extremely slowly in the case of metals. Dense sampling of the Brillouin zone, required for high accuracy, is computationally expensive, especially when implementing hybrid functionals or perturbative expansions in density functional theory (DFT) [52]. High accuracy is important because the energies of competing phases are often similar and even small errors can affect the prediction of stable materials.

Methods for **k**-point selection have not changed much since Monkhorst and Pack published their influential paper over 40 years ago [53]. Their method was quickly accepted by the community due to its simplicity and ability to generalize previous methods [54,55]. Sampling methods that improve upon Monkhorst-Pack (MP) grids have been far less prevalent [1,56–58].

In this paper, we compare the **k**-point selection method promoted by Wisesa, McGill, and Mueller [1] (WMM) to the standard MP grids and to another common method in the alloy community, which we refer to as *simultaneously commensurate* (SC) grids. This paper serves to reinforce and quantify the claims made by WMM, as applied to calculations typically used for alloys and for some high-throughput studies.

2. Background

Over the past 40 years, only a few **k**-point selection methods have been proposed in the literature [1,53–57]. Many of these so-called special point methods have focused on selecting points that accurately determined the mean value of a periodic function defined over the Brillouin zone because the integral of a periodic function over one period is simply its mean value. Other factors that have been considered in developing special point methods are selection of grids with a consistent density in each direction and full exploitation of symmetry.

Baldereschi introduced the *mean-value point* of the Brillouin zone [54], the first special point method. In this approach, the periodic function to be integrated is written as a Fourier expansion:

$$f(\mathbf{k}) = \sum_{n=0}^{\infty} c_n e^{i\mathbf{k}\cdot\mathbf{R}_n}, \tag{1}$$

where $\mathbf{k}$ is the wavevector, c_n is the n-th expansion coefficient, and the sum is over over all lattice points $\mathbf{R}_n$. Baldereschi noted that the integral of $f(\mathbf{k})$ within the first Brillouin zone (i.e., over one period of $f(\mathbf{k})$), is proportional to the leading coefficient, c_0, in the Fourier expansion,

$$\int_{\mathrm{BZ}} f(\mathbf{k})\,d\mathbf{k} = \frac{(2\pi)^3}{\Omega} c_0, \tag{2}$$

where Ω is the volume of the reciprocal cell. He replaced the analytic

---

* Corresponding author.
  E-mail address: wiley.s.morgan@gmail.com (W.S. Morgan).

integral of the periodic function with a numeric integral (sum over j in Eq. (3))—equivalent in the limit of infinite sampling points—and replaced the periodic function with its infinite Fourier expansion (sum over n in Eq. (3)):

$$
\begin{aligned}
\int_{BZ} f(\mathbf{k}) &= \sum_{j=0}^{\infty} w_j f(\mathbf{k}_j) \\
&= \sum_{j=0}^{\infty} w_j \sum_{n=0}^{\infty} c_n e^{i\mathbf{k}_j \cdot \mathbf{R}_n} \\
&= \sum_{j=0}^{\infty} w_j (c_0 + c_1 e^{i\mathbf{k}_j \cdot \mathbf{R}_1} + \ldots) \\
&= \sum_{j=0}^{\infty} w_j c_0 + \sum_{j=0}^{\infty} w_j c_1 e^{i\mathbf{k}_j \cdot \mathbf{R}_1} + \ldots,
\end{aligned}
\tag{3}
$$

where w_j is the integration weight of the j-th $\mathbf{k}$-point. In the final step of Eq. (3), each term (sum over j) is a numeric integral of the n-th basis function in the Fourier expansion of $f(\mathbf{k})$ (denoted as I_n in what follows). Baldereschi's method selected $\mathbf{k}$-points so that the leading terms after c_0 integrate to zero:

$$
\begin{aligned}
\int_{BZ} f(\mathbf{k}) &= \sum_{j=0}^{\infty} w_j c_0 + \sum_{j=0}^{\infty} w_j c_1 e^{i\mathbf{k}_j \cdot \mathbf{R}_1} + \\
&\quad \sum_{j=0}^{\infty} w_j c_2 e^{i\mathbf{k}_j \cdot \mathbf{R}_2} + \ldots \\
&= I_0 + I_1^{0} + I_2^{0} + \mathcal{O}(I_3), \\
&\approx c_0 \sum_j w_j.
\end{aligned}
$$

This is an accurate approximation when the Fourier coefficients converge rapidly to zero, as is the case with insulators and semiconductors. Baldereschi's approximation is ineffective for metals because the integral over the occupied parts of the band structure has discontinuities, and the Fourier series converges very slowly.

Chadi and Cohen extended the mean-value point by introducing *sets* of $\mathbf{k}$-points whose weighted sum eliminated the contribution of a greater number of leading basis functions [55]. Their sets of $\mathbf{k}$-points could be made as dense as desired.

The most popular $\mathbf{k}$-point selection method was created by Monkhorst and Pack [53] (MP). They established a grid of points that generalized both the mean-value point of Baldereschi and its extension by Chadi and Cohen and which was equivalent to points used by Janak et al. [59] MP grids are given by the relation

$$
\mathbf{k}_{prs} = u_p \mathbf{b}_1 + u_r \mathbf{b}_2 + u_s \mathbf{b}_3
\tag{4}
$$

where $\mathbf{b}_1$, $\mathbf{b}_2$, and $\mathbf{b}_3$ are the reciprocal lattice vectors, $u_p = (2p-q-1)/2q$ for $p = 1, 2, \ldots, q$, and q an integer that determines the grid density. The same relation holds for u_r and u_s. In other words, the generating vectors of MP grids are simply integer divisions of the reciprocal lattice vectors.

Froyen generalized the MP points, which he called *Fourier quadrature points*, by eliminating the restriction that the vectors that defined the grid be parallel to the reciprocal lattice vectors [56]. However, he did require the grid to be commensurate with the reciprocal lattice and to have the full point-group symmetry of the crystal.

Moreno and Soler [57] introduced the idea of searching for $\mathbf{k}$-point grids with the fewest points for a given length cutoff—a parameter that characterized the quality of the grid and was closely related to the $\mathbf{k}$-point density. Their method constructs superlattices of the real-space primitive lattice. The *dual* of the superlattice vectors form the $\mathbf{k}$-point grid generating vectors. By selecting superlattices that maximize the minimum distance between lattice points (i.e., by choosing fcc-like superlattices), they obtain $\mathbf{k}$-point grids that are bcc-like. Grids that are bcc-like have the smallest integration errors at a given $\mathbf{k}$-point density. (This is evident in Fig. 6.) Moreno and Soler further improved Brillouin
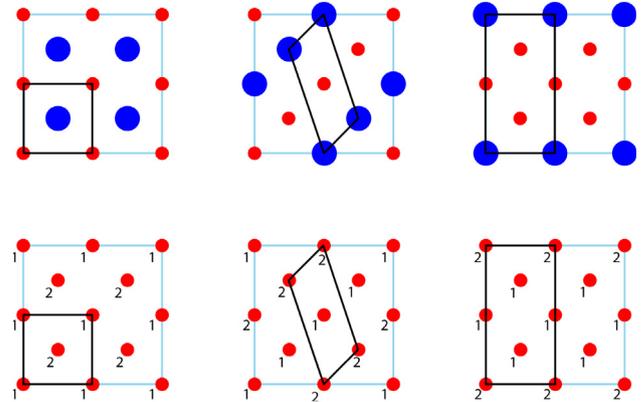
Fig. 1. In order to isolate the effect of the Brillouin zone shape and size on total energy error when comparing crystal structures of different shapes and sizes (top row), the energy of supercells (bottom row) crystallographically equivalent to single element, primitive cells were compared. The total energy per atom should be the same for all equivalent cells.

zone sampling by finding the offset of the origin that maximized the symmetry reduction of the grid.

In their recent paper, WMM point out that the lack of popularity of Moreno and Soler's approach is due to the computational expense of calculating many Froyen grids and searching for the ones with the highest symmetry reduction. They used the term *Generalized Monkhorst-Pack* (GMP) grids to refer to Froyen grids with the highest symmetry reduction for a given $\mathbf{k}$-point density. We refer to these grids as *Generalized Regular* (GR) grids since they are simply generalizations of the regular grids used in finite element, finite difference, and related methods. WMM precalculated the grids, and stored the ones with the
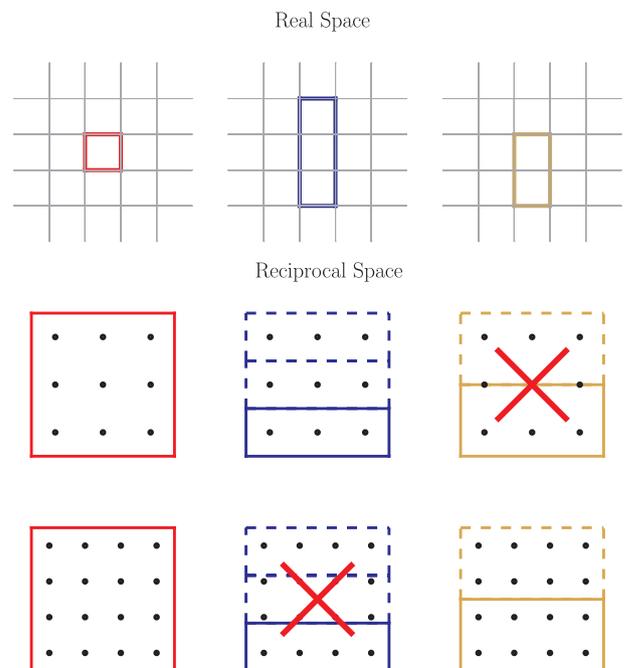
Fig. 2. An example of simultaneously commensurate grids. The cells for each crystal are shown in both real and reciprocal space. In reciprocal space, we include two $\mathbf{k}$-point grids of different density. Simultaneously commensurate grids eliminate systematic $\mathbf{k}$-point error (between two commensurate structures) by using the same grid for both the parent cell (red cell) and the supercells (yellow and blue). However, some grids may not be allowed (crossed out) for a given supercell because they are incommensurate with the reciprocal cell. (For interpretation of the references to color in this figure legend, the reader is referred to the web version of this article.)
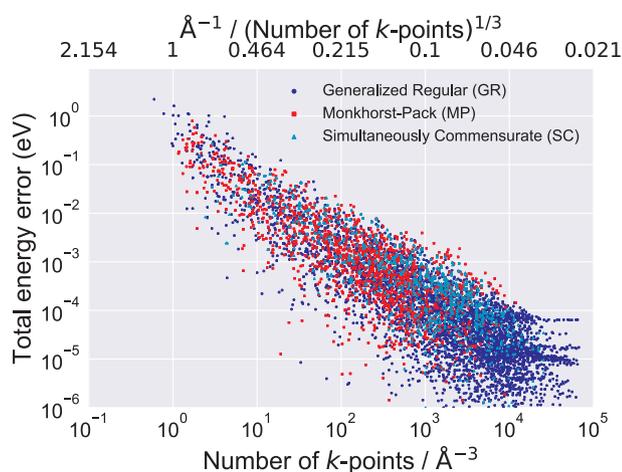
Fig. 3. Total energy convergence by grid type. Note that the size of the convergence envelope gets bigger with higher **k**-point densities.

Fig. 4. Total energy convergence with respect to the irreducible **k**-point density. By looking at the irreducible **k**-point density the efficiency of the different grids can be distinguished. Loess smoothing was also employed to determine the average efficiency of the grids.

highest symmetry reduction in a database that can be accessed via an internet request.

3. Methods

We compare the total energy errors of MP, SC, and GR grids for different **k**-point densities over calculations of nine different elements (all of which are metallic), many cell shapes, and cell sizes from 1 to 14 atoms. In total we compare errors across more than 7000 total energy calculations. One **k**-point grid is considered superior to another if it requires a smaller irreducible **k**-point density to reach a specific accuracy target (for example 10^{-3} eV/atom). The method that requires the smallest irreducible **k**-point density is the one we regard as best suited for high throughput and machine learning applications.

To isolate error arising from **k**-point integration, the different cells were crystallographically equivalent to single element, primitive cells, as illustrated in Fig. 1. We did this to study how **k**-point error depends on the Brillouin zone shape and size; this is an important consideration in high-throughput studies where total energy differences between competing phases are critical.

The grid types we compared were MP grids (generated by AFLOW's algorithm [32]), SC grids [56] (examples of SC grids can be found in Fig. 2, details of SC grid generation can be found in the appendix), and GR grids (generated by querying WMM's **k**-point server) [60]. We ran DFT calculations using the Vienna Ab-initio Simulation Package (VASP) [61–64] on nine monoatomic systems—Al, Pd, Cu, W, V, K, Ti, Y, and Re—using PAW PBE pseudopotentials [65,66]. The supercells of cubic systems varied between 1 and 11 atoms per cell, while the hexagonal close packed (HCP) systems had 2–14 atoms per cell. We used VASP 4.6 for all calculations[1]. For MP and SC grids the target number of **k**-points extended from 10 to 10,000 unreduced **k**-points The range of **k**-points for GR grids was 4–150,000 **k**-points[2].

The converged total energy, the energy taken as the error-free "solution" in our energy convergence comparisons, was the calculation with the highest **k**-point density for each system. Because MP and SC grids are difficult to generate at comparable densities, GR grids were used to generate the converged total energy.

---

[1] For SC grids an independent k-point folding algorithm was used due to an occasional bug in VASP 4.6's folding algorithm. This bug has been fixed in version 6 of VASP.

[2] Calculations with MP grids with more than about 10,000 unreduced points were not used. These calculations were problematic due to a number of problems, including memory constraints and errors during the k-point folding.
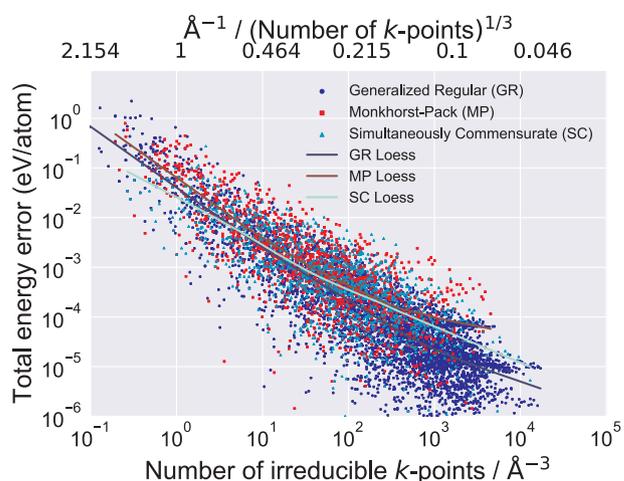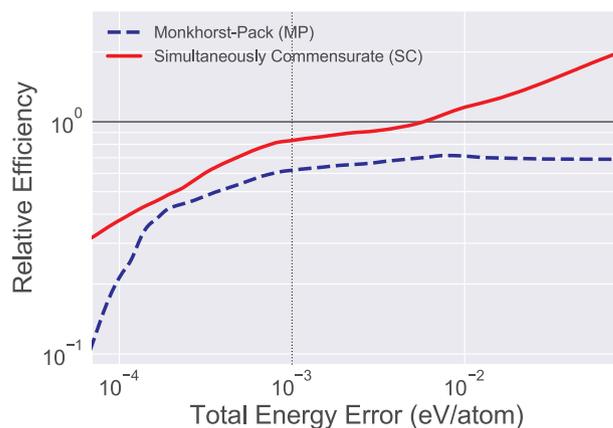
Fig. 5. Relative grid efficiency. Along the y-axis are the ratios of the MP and SC efficiencies compared to the GR grid efficiency (black horizontal line at 10^0). Total energy error (per atom) is plotted along the x-axis and decreases to the left. MP and SC grids are generally less efficient than GR grids: at a target accuracy of 1 meV/atom, MP grids are 60%, and SC grids are 20%, less efficient.

4. Results

In Fig. 3, we show the convergence for the MP, SC, and GR grids with respect to the **k**-point density, i.e., **k**-points/Å^{-3}. The first thing to note is the large spread in the convergence. This spread reduces the reliability of high-throughput databases and is perhaps higher than one might expect. Note that the size of the total energy convergence envelope (variance) gets bigger with increasing **k**-point densities. Additionally it can be seen that each method has the same variance at all **k**-point densities.

In order to quantify the efficiency of GR grids relative to SC and MP grids, we studied the rate of energy convergence with respect to the irreducible **k**-point density, i.e., the number of *irreducible* **k**-points divided by the volume of the reciprocal cell in Å^{-3} (shown in Fig. 4). Given the amount of scatter in the plot, we performed loess regression to create trend lines for each grid type.

The efficiency of a **k**-point grid is proportional to the irreducible **k**-point density required to reach a given accuracy. Comparisons of efficiencies were made by taking the ratio of the GR trend line to the SC and MP trend lines of Fig. 5. At accuracies higher than 5 meV/atom, GR grids are more efficient (averaged over many structures) than MP and SC grids. As an example, at a target accuracy of 1 meV/atom, the GR grids are 20%

more efficient than SC grids and 60% more efficient than MP grids.

It should be noted that in both Figs. 4 and 5 that MP grids appear to perform worse at higher densities than at lower densities. Our statistical analysis has indicated that this behavior is not statistically significant and likely results from data scarcity for MP grids at high densities. We believe that with sufficient data for MP grids at these densities the trend line would continue to run roughly parallel to the GR line across all densities. However, due to the computational expense of generating MP grids at such densities we have been unable to demonstrate this.

5. Discussion

The erratic convergence of total energy for metals is attributed principally to the Fermi surface. Integrating over the occupied portions of the band structure is equivalent to integrating a discontinuous band structure over the Brillouin zone; the rapid, monotonic convergence observed for insulators and semiconductors is lost because of the surface of discontinuities.

It is perhaps surprising how much the error varies at a given **k**-point density. The implication is that, when generating databases of total energies, relatively high **k**-point densities will be required for accurate comparisons. For example, in Fig. 4, **k**-point densities as low as 10s of **k**-points/$Å^{-3}$ achieve 10^{-3} eV/atom error for some structures, but to be certain that *all* structures are converged to the same accuracy densities as high as 5000 **k**-points/$Å^{-3}$ are necessary. Given the spread in the data we recommend that a target density of 5000 **k**-points/$Å^{-3}$ be used to reliably achieve accuracies of 10^{-3} eV/atom for metals. However, should another accuracy be desired, one can simply follow the top edge of the distribution of points in Fig. 3 to the desired accuracy and read off the corresponding density.

For reference: a **k**-point density of 5000 **k**-points/$Å^{-3}$ corresponds to a linear **k**-point density of 0.058 $Å^{-1}$ (common input scheme for CASTEP or newer versions of VASP, KSPACING in the INCAR file). This is equivalent to the following Monkhorst-Pack grids or "**k**-point per reciprocal atom" (KPPRA) settings for a few pure elements:

Element	Cell divisions	KPPRA
W	$43 \times 43 \times 43$	80,000
Cu	$48 \times 48 \times 48$	110,500
Al	$43 \times 43 \times 43$	80,000
K	$26 \times 26 \times 26$	17,500
Ti (2 atoms, hcp)	$41 \times 41 \times 21$	18,000
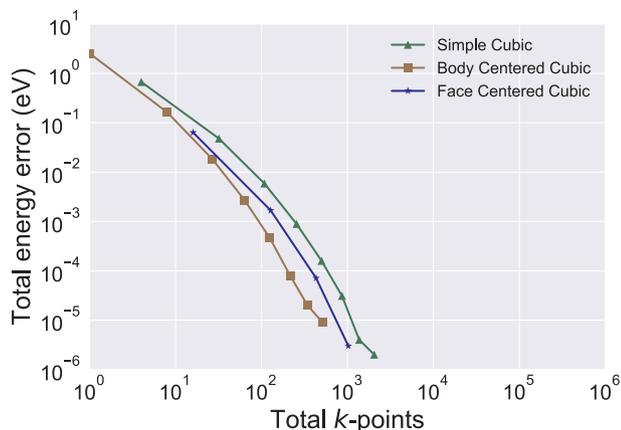
Likely these high numbers will be surprising to most DFT practitioners—indeed, the current authors found them so—but this is the message of Fig. 4 if one wants to be fully converged in all cases, and not just on average. The large scatter in the errors for a given density imposes this large penalty on the practitioner who wishes to have fully converged calculations. The need for high densities when using a regular grid for DFT calculations of metallic systems highlights the need for development of adaptive techniques that can mitigate the deleterious effects of a discontinuous integrand (i.e., the existence of a Fermi surface.)

In our tests of GR grids, we also observed large spread in the energy convergence of insulators, rather than the typical monotonic convergence observed for MP grids. This happens because GR grids are not restricted to a single Bravais lattice type. Grids of different lattice types will have different packing fractions and thus converge at different rates. Fig. 6 shows the energy convergence rate of primitive silicon for three Bravais lattice types; the convergence is monotonic for each type. As expected, body-centered cubic grids have the fastest convergence. This is because bcc lattices have the highest packing fraction when Fourier transformed (becoming fcc). If grids of multiple Bravais lattice types are used, as happens for GR grids obtained by querying WMM's **k**-point server, spread in the energy convergence is introduced. To demonstrate that erratic convergence for metals is not merely due to mixing grids of multiple Bravais lattice types, we include Fig. 7. The figure also demonstrates that the grid type, i.e., bcc, fcc, or sc, has no effect on the convergence.

6. Conclusion

GR grids are not intrinsically better than SC or MP grids—that is, they do not converge more rapidly as a function of **k**-point density. They are more efficient because they typically have better symmetry reduction than MP or SC grids, reducing the computational effort required for GR grids. Also, with GR grids one may increase the **k**-point density in smaller increments because the set of possible grids (and thus **k**-point densities) is larger than the sets of possible grids for SC and MP.

Our tests over more than 7000 structures of varying cell sizes, shapes, and **k**-point densities demonstrate how erratic **k**-point convergence is for metals, and how wide the variance can be at a given **k**-point density, and how this variance grows with increasing **k**-point densities. These facts should be considered when generating computational materials databases since greater errors may result from not

Fig. 6. Convergence for silicon by Bravais lattice type of the **k**-point grid. The energy convergence remains smooth for GR grids as long as the grid is of a single Bravais lattice type. Otherwise, some spread in the energy convergence, similar to that observed for metals, is introduced.
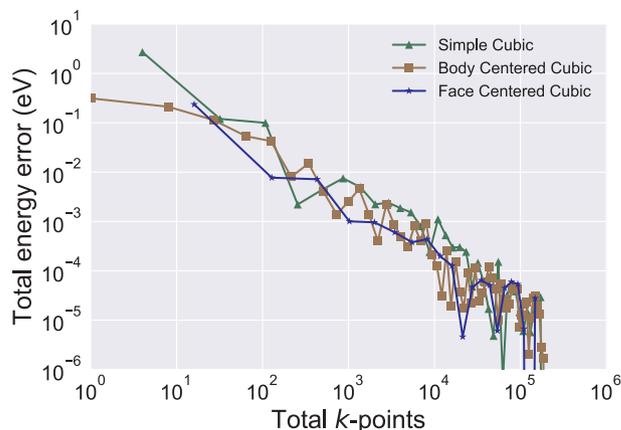
Fig. 7. (Color online) Convergence of aluminum by Bravais lattice type of the **k**-point grid. Jaggedness and spread in the energy convergence remains for GR grids even after separating the grids by Bravais lattice type.

using enough **k**-points for a target accuracy. Using GR grids for non-metals may result in unexpected scatter; when smooth convergence is desired, we advise that GR grids of a single Bravais lattice type be utilized.

Acknowledgments

The authors are grateful to Shane Reese who helped with the loess

Appendix A. Simultaneously commensurate grid construction

A *simultaneously commensurate* (SC) grid is useful for calculating formation enthalpies when the target structure is a derivative superstructure of a parent structure. (Obviously this is a convenient method when computing enthalpies for cluster expansion studies because the training structures are superstructures of the parent.) When SC grids are used, the absolute convergence with respect to **k**-point density is not faster than for other grids but the *relative convergence* can be faster because of error cancellation—both the parent structure and the derivative superstructure have exactly the same grid. The idea is illustrated in Fig. 8. In panel (a) we divide up the reciprocal unit cell of the parent lattice (red[3] parallelogram) into a uniform grid of **k**-points (blue points). We then place the same grid from the parent cell on the supercell, as in panel (b). If we have chosen a SC grid, it is clearly periodic for the supercell as well as the parent. Only those grids that are commensurate with both the parent cell and supercell can be used to integrate both cells. Fig. 9 shows an example of an incommensurate grid. When the grid of the parent cell is placed over the reciprocal cell of the supercell, the grid is *not periodic*—translations of the supercell (dotted lines) are sampled differently by the grid.

For our crystals that have cubic parent cells, an initial set of commensurate bcc, fcc, and sc grids were generated. A subset of those grids that were commensurate with each supercell were used to do calculations of the various crystal structures. For hexagonal crystals, a similar procedure was followed except only hexagonal grids were used.
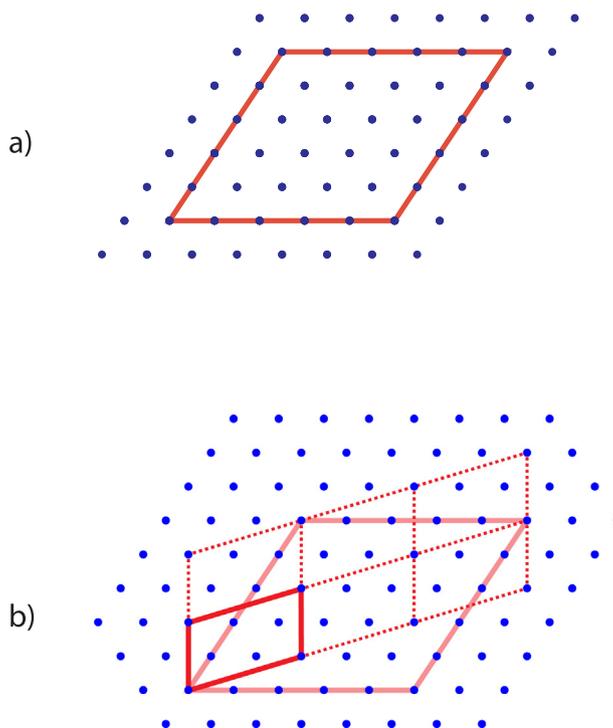
Fig. 8. (Color online) An example of a SC grid. Panel a): the selected grid (blue points) is commensurate with the reciprocal cell (red parallelogram) of the parent cell. Panel b): it can be seen that the grid is also commensurate with the reciprocal unit cell of the supercell (smaller parallelogram). (Dotted lines indicate translations of the supercell.) The **k**-point grid is the same in each translation of the supercell.

---

[3] For interpretation of color in Fig. 8, the reader is referred to the web version of this article.
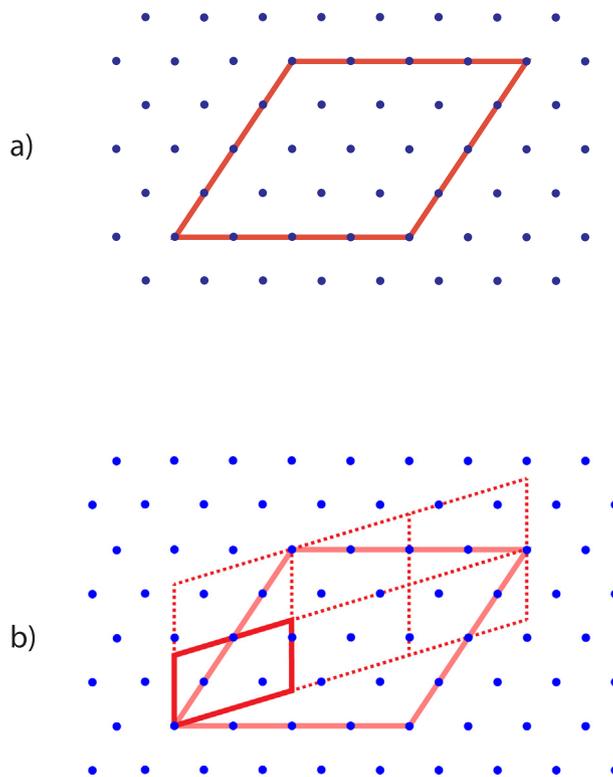
Fig. 9. (Color online) An example of a SC grid (blue dots) that is not commensurate with both the reciprocal unit cell of the parent cell and the reciprocal unit cell of the supercell. Panel a): the chosen grid is commensurate with the parent cell (red parallelogram). Panel b): the **k**-point grid is not commensurate with the super-cell—it is not periodic; the grid is not the same in each translational copy (dotted lines) of the supercell.

Appendix B. Supplementary material

Supplementary data associated with this article can be found, in the online version, at https://doi.org/10.1016/j.commatsci.2018.06.031.

References

[1] P. Wisesa, K.A. McGill, T. Mueller, Phys. Rev. B 93 (2016) 155109.
[2] J. Greeley, T.F. Jaramillo, J. Bonde, I. Chorkendorff, J.K. Nørskov, Nat. Mater. 5 (2006) 909.
[3] R. Gautier, X. Zhang, L. Hu, L. Yu, Y. Lin, T.O. Sunde, D. Chon, K.R. Poeppelmeier, A. Zunger, Nat. Chem. 7 (2015) 308.
[4] A.O. Oliynyk, A. Mar, Acc. Chem. Res. (2017).
[5] H. Chen, G. Hautier, A. Jain, C. Moore, B. Kang, R. Doe, L. Wu, Y. Zhu, Y. Tang, G. Ceder, Chem. Mater. 24 (2012) 2009.
[6] G. Hautier, A. Jain, S.P. Ong, B. Kang, C. Moore, R. Doe, G. Ceder, Chem. Mater. 23 (2011) 3495.
[7] C. Jahne, C. Neef, C. Koo, H.-P. Meyer, R. Klingeler, J. Mater. Chem. A 1 (2013) 2856.
[8] T. Moot, O. Isayev, R.W. Call, S.M. McCullough, M. Ze-maitis, R. Lopez, J.F. Cahoon, A. Tropsha, Mater. Discov. 6 (2016) 9.
[9] U. Aydemir, J.-H. Pohls, H. Zhu, G. Hautier, S. Bajaj, Z.M. Gibbs, W. Chen, G. Li, S. Ohno, D. Broberg, et al., J. Mater. Chem. A 4 (2016) 2461.
[10] H. Zhu, G. Hautier, U. Aydemir, Z.M. Gibbs, G. Li, S. Bajaj, J.-H. Pohls, D. Broberg, W. Chen, A. Jain, et al., J. Mater. Chem. C 3 (2015) 10554.
[11] W. Chen, J.-H. Pohls, G. Hautier, D. Broberg, S. Bajaj, U. Aydemir, Z.M. Gibbs, H. Zhu, M. Asta, G.J. Snyder, et al., J. Mater. Chem. C 4 (2016) 4414.
[12] G. Ceder, Y.-M. Chiang, D. Sadoway, M. Aydinol, Y.-I. Jang, B. Huang, Nature 392 (1998) 694.
[13] F. Yan, X. Zhang, G.Y. Yonggang, L. Yu, A. Nagaraja, T.O. Mason, A. Zunger, Nat. Commun. 6 (2015).
[14] D. Bende, F.R. Wagner, O. Sichevych, Y. Grin, Angew. Chem. 129 (2017) 1333.
[15] A. Mannodi-Kanakkithodi, A. Chandrasekaran, C. Kim, T.D. Huan, G. Pilania, V. Botu, R. Ramprasad, Mater. Today (2017).
[16] S. Sanvito, C. Oses, J. Xue, A. Tiwari, M. Zic, T. Archer, P. Tozman, M. Venkatesan, M. Coey, S. Curtarolo, Sci. Adv. 3 (2017) e1602241.
[17] H. Yaghoobnejad Asl, A. Choudhury, Chem. Mater. 28 (2016) 5029.
[18] G. Hautier, A. Miglio, G. Ceder, G.-M. Rignanese, X. Gonze, Nat. Commun. 4 (2013) 2292.
[19] A. Bhatia, G. Hautier, T. Nilgianskul, A. Miglio, J. Sun, H.J. Kim, K.H. Kim, S. Chen, G.-M. Rignanese, X. Gonze, et al., Chem. Mater. 28 (2015) 30.
[20] G.H. Johannesson, T. Bligaard, A.V. Ruban, H.L. Skriver, K.W. Jacobsen, J.K. Nørskov, Phys. Rev. Lett. 88 (2002) 255506.

[21] D.P. Stucke, V.H. Crespi, Nano Lett. 3 (2003) 1183.
[22] S. Curtarolo, D. Morgan, G. Ceder, Calphad 29 (2005) 163.
[23] S.F. Matar, I. Baraille, M. Subramanian, Chem. Phys. 355 (2009) 43.
[24] G. Ceder, G. Hautier, A. Jain, S.P. Ong, MRS Bull. 36 (2011) 185.
[25] A.N. Sokolov, S. Atahan-Evrenk, R. Mondal, H.B. Akker-man, R.S. Sanchez-Carrera, S. Granados-Focil, J. Schrier, S.C. Mannsfeld, A.P. Zoombelt, Z. Bao, et al., Nat. Commun. 2 (2011) 437.
[26] Z.W. Ulissi, M.T. Tang, J. Xiao, X. Liu, D.A. Torelli, M. Karamad, K. Cummins, C. Hahn, N.S. Lewis, T.F. Jaramillo, et al., ACS Catal. 7 (2017) 6600.
[27] O. Levy, R.V. Chepulskii, G.L. Hart, S. Curtarolo, JACS 132 (2009) 833.
[28] X. Ma, G. Hautier, A. Jain, R. Doe, G. Ceder, J. Electrochem. Soc. 160 (2013) A279.
[29] K. Yang, W. Setyawan, S. Wang, M.B. Nardelli, S. Curtarolo, Nat. Mater. 11 (2012) 614.
[30] H. Chen, G. Hautier, G. Ceder, JACS 134 (2012) 19619.
[31] S. Kirklin, B. Meredig, C. Wolverton, Adv. Energy Mater. 3 (2013) 252.
[32] S. Curtarolo, W. Setyawan, G.L. Hart, M. Jahnatek, R.V. Chepulskii, R.H. Taylor, S. Wang, J. Xue, K. Yang, O. Levy, et al., Comput. Mater. Sci. 58 (2012) 218.
[33] J.E. Saal, S. Kirklin, M. Aykol, B. Meredig, C. Wolverton, JOM 65 (2013) 1501.
[34] A. Jain, S.P. Ong, G. Hautier, W. Chen, W.D. Richards, S. Dacek, S. Cholia, D. Gunter, D. Skinner, G. Ceder, et al., APL Mater. 1 (2013) 011002.
[35] S.L. Digabel, C. Tribes, C. Audet, NOMAD User Guide. Tech. Rep. G-2009-37, Les cahiers du GERAD, Quebec, Canada, 2009.
[36] D.D. Landis, J.S. Hummelshøj, S. Nestorov, J. Greeley, M. Dulak, T. Bligaard, J.K. N0rskov, K.W. Jacobsen, Comput. Sci. Eng. 14 (2012) 51.
[37] J. Hachmann, R. Olivares-Amaya, S. Atahan-Evrenk, C. Amador-Bedolla, R.S. Sanchez-Carrera, A. GoldParker, L. Vogt, A.M. Brockway, A. Aspuru-Guzik, J. Phys. Chem. Lett. 2 (2011) 2241.
[38] J.S. Hummelshøj, F. Abild-Pedersen, F. Studt, T. Bligaard, J.K. Nørskov, Angew. Chem. 124 (2012) 278.
[39] M. De Jong, W. Chen, H. Geerlings, M. Asta, K.A. Persson, Sci. Data 2 (2015).
[40] M. De Jong, W. Chen, T. Angsten, A. Jain, R. Notestine, A. Gamst, M. Sluiter, C.K. Ande, S. Van Der Zwaag, J.J. Plata, et al., Sci. Data 2 (2015) 150009.
[41] L. Cheng, R.S. Assary, X. Qu, A. Jain, S.P. Ong, N.N. Rajput, K. Persson, L.A. Curtiss, J. Phys. Chem. Lett. 6 (2015) 283.
[42] R. Gomez-Bombarelli, J. Aguilera-Iparraguirre, T.D. Hirzel, D. Duvenaud, D. Maclaurin, M.A. Blood-Forsythe, H.S. Chae, M. Einzinger, D.-G. Ha, T. Wu, et al., Nat. Mater. 15 (2016) 1120.
[43] E.M. Chan, Chem. Soc. Rev. 44 (2015) 1653.
[44] T. Tada, S. Takemoto, S. Matsuishi, H. Hosono, Inorg. Chem. 53 (2014) 10347.

[45] G. Pilania, C. Wang, X. Jiang, S. Rajasekaran, R. Ramprasad, Sci. Rep. 3 (2013).
[46] J. Yan, P. Gorai, B. Ortiz, S. Miller, S.A. Barnett, T. Mason, V. Stevanovic, E.S. Toberer, Energy Environ. Sci. 8 (2015) 983.
[47] R. Ramakrishnan, P.O. Dral, M. Rupp, O.A. Von Lilienfeld, Sci. Data 1 (2014) 140022.
[48] J. Hachmann, R. Olivares-Amaya, A. Jinich, A.L. Ap-pleton, M.A. Blood-Forsythe, L.R. Seress, C. Roman-Salgado, K. Trepte, S. Atahan-Evrenk, S. Er, et al., Energy Environ. Sci. 7 (2014) 698.
[49] L.-C. Lin, A.H. Berger, R.L. Martin, J. Kim, J.A. Swisher, K. Jariwala, C.H. Rycroft, A.S. Bhown, M.W. Deem, M. Haranczyk, et al., Nat. Mater. 11 (2012) 633.
[50] R. Armiento, B. Kozinsky, G. Hautier, M. Fornari, G. Ceder, Phys. Rev. B 89 (2014) 134103.
[51] O. Senkov, J. Miller, D. Miracle, C. Woodward, Nat. Commun. 6 (2015).
[52] K. Berland, C. Persson, Comput. Mater. Sci. 134 (2017) 17.
[53] H.J. Monkhorst, J.D. Pack, Phys. Rev. B 13 (1976) 5188.
[54] A. Baldereschi, Phys. Rev. B 7 (1973) 5212.
[55] D.J. Chadi, M.L. Cohen, Phys. Rev. B 8 (1973) 5747.
[56] S. Froyen, Phys. Rev. B 39 (1989) 3168.
[57] J. Moreno, J.M. Soler, Phys. Rev. B 45 (1992) 13891.
[58] E. Cances, V. Ehrlacher, D. Gontier, A. Levitt, D. Lombardi, Available from: < arXiv:1805.07144 > .
[59] J. Janak, Computational Methods in Band Theory, Springer, 1971, pp. 323–339.
[60] http://muellergroup.jhu.edu/K-Points.html.
[61] G. Kresse, J. Hafner, Phys. Rev. B 47 (1993) 558.
[62] G. Kresse, J. Furthmuller, Comput. Mater. Sci. 6 (1996) 15.
[63] G. Kresse, J. Hafner, Phys. Rev. B 49 (1994) 14251.
[64] G. Kresse, J. Furthmuller, Phys. Rev. B 54 (1996) 11169.
[65] P.E. Blochl, Phys. Rev. B 50 (1994) 17953.
[66] G. Kresse, D. Joubert, Phys. Rev. B 59 (1999) 1758.